

Supplementary Information

Emulating Synaptic Plasticity with Poly[N-(3-(9H-carbazol-9-yl)propyl)methacrylamide] Memristor

Yadu Ram Panthi^{a,b}, Ambika Pandey^{a,b}, Adriana Šturcová^a, Drahomír Výprachtický^a, Stephen H. Foulger^{c,d} and Jiří Pflieger^{a,†}

^a Institute of Macromolecular Chemistry, Czech Academy of Sciences, Heyrovského nám. 2, 16206, Prague 6, Czech Republic.

^b Faculty of Mathematics and Physics, Charles University, Ke Karlovu 3, Prague 2, Czech Republic.

^c Center for Optical Materials Science and Engineering Technology (COMSET), Department of Materials Science and Engineering, Clemson University, Clemson, SC 29634, USA.

^d Department of Bioengineering, Clemson University, Clemson, SC 29634, USA.

† Correspondence

Table of Contents

Description	Page no.
Table S1. Calculation of Schottky barrier	7
Figure S1. Schematic of the device used for spectro-electrochemical measurement	2
Figure S2. AFM images of PCaPMA films cast on ITO/ glass substrate	2
Figure S3. Series of I–V characteristics of ITO PCaPMA Au memristive device	3
Figure S4. Pulse-controlled synaptic weight modulation in ITO PCaPMA Al device	3
Figure S5. Thickness dependence and sample-to-sample reproducibility of potentiation	4
Figure S6 Impact of number of trigger pulses on device potentiation and non-volatile characteristics	4
Figure S7. Progression of STP to LTP and the memory transition	5
Figure S8. Schematic of Pavlovian learning algorithm: stimulus-responsive paradigm	6
Figure S9. Simulation of pair-pulse facilitation/ depression (PPF/D)	6
Figure S10. Band-diagram of the ITO PCaPMA Au or Al devices.	7
Figure S11. In-situ Raman spectroscopy under applied voltage (laser excitation at 488 nm, layer thickness of 550 nm)	7-8
Figure S12. In-situ Raman spectroscopy under applied voltage (laser excitation at 532 nm, layer thickness of 175 nm)	8
Figure S13. In-situ fluorescence emission spectroscopy under applied voltage	9
References	9

A. Spectro-electrochemical (SEC) Measurement

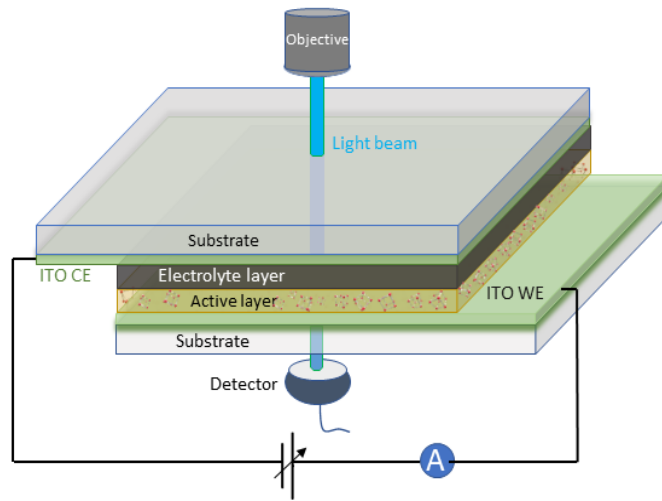


Fig. S1: Diagram of a device with glass | ITO | active layer | electrolyte layer | ITO | glass structure used for the spectro-electrochemical measurements and the experimental setup used.

B. Atomic Force Microscopy

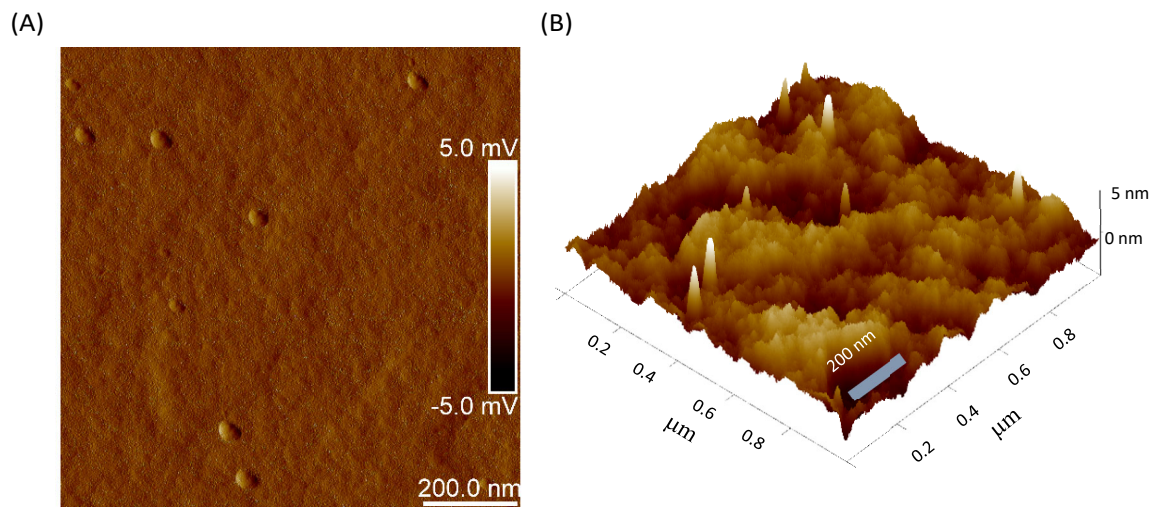


Fig. S2: AFM images of PCaPMA films spin-cast on an ITO/glass substrate. A) 2D scan with amplitude sensor, B) 3D scan with height sensor.

C. Sweep-based Electrical Characterization

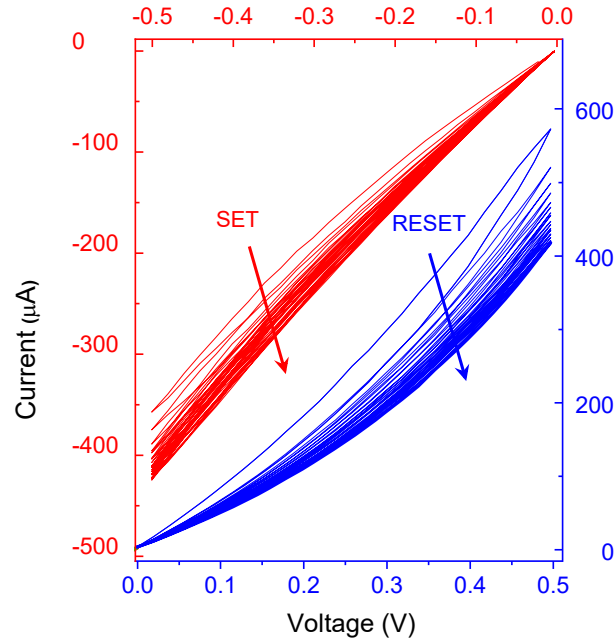


Fig. S3: Sequential I-V characteristics of the ITO | PCaPMA | Au memristive device recorded during the sequential voltage sweeps between 0 and ± 0.5 V (sweep rate: 0.5 V/s) indicating the multilevel memory properties.

Voltage-induced resistance changes were characterized by the measurement of current-voltage (I-V) characteristics in an ITO | PCaPMA (30-100 nm) | Al or Au devices. The voltage sweep spanned from 0 to -0.5 V and then reversed back to 0 V, at a rate of 0.5 V/s, and 20 scans showed an analog increase in device conductance. This behavior emulates the long-term potentiation (LTP) as a prolonged strengthening of the synapse. The reverse sweeps of the same magnitude decrease the conductance similar to the long-term depression (LTD), which mimics the weakening of the synaptic connection.

D. Conductance Modulation in ITO | PCaPMA | Al Device

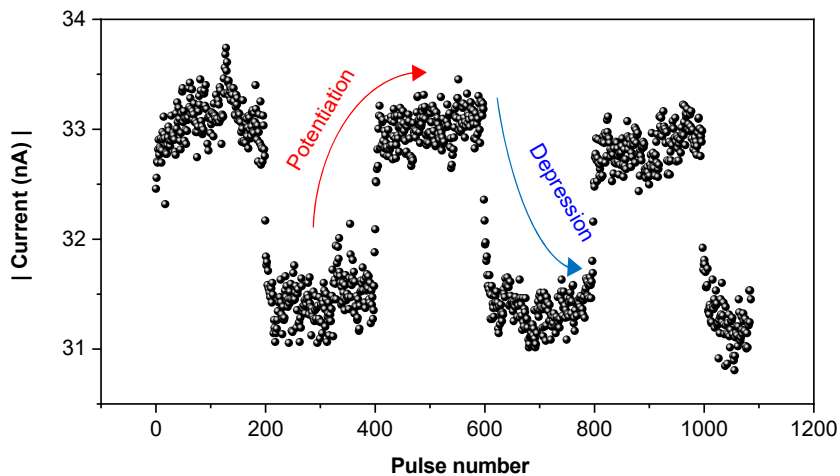


Fig. S4: Pulse-controlled synaptic weight modulation in ITO | PCaPMA | Al device, comprising of 200 consecutive potentiation pulses (amplitude: - 500 mV, pulse width: 10 ms), followed by 200 successive depression pulses (+500 mV; 10 ms), each followed with a reading pulse (-50 mV, 50 ms duration) at 20 ms delay after each potentiation and depression pulses.

E. Thickness dependence and sample-to-sample reproducibility of potentiation

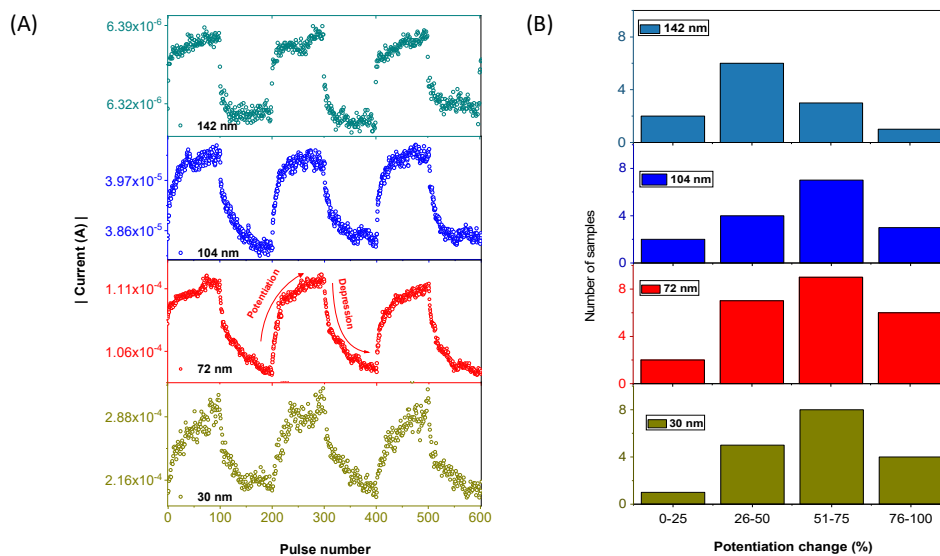


Fig. S5: A) Thickness-dependent P/D changes during three subsequent cycles, each with 100 potentiation only pulses followed by the same number of depressions only pulses. Thickness shown in the legends. B) The statistical distribution of conductance changes during potentiation/depression cycles in 70 randomly selected cells from two polymer batches with active layer thickness specified in legends.

F. Impact of Number of Triggers on Device Potentiation and Non-volatile Characteristics

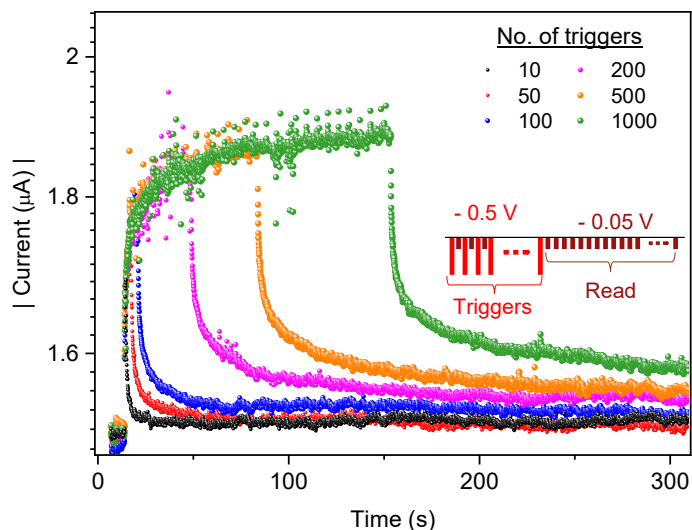


Fig. S6: Impact of number of triggers on device potentiation and non-volatile characteristics in ITO | PCaPMA | Au device. The data points represent readings obtained both during triggering (exponential increase) and after excitation (exponential decrease). Trigger pulses: -500 mV, 20 ms and read pulses: -50 mV, 50 ms. The experiment was carried out in the active area of 0.15 mm².

G. Short-term to Long-term Memory Transition

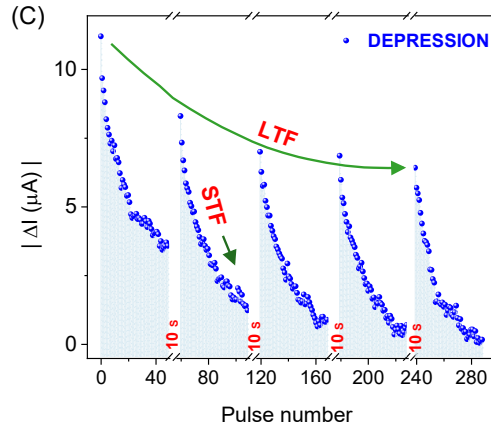
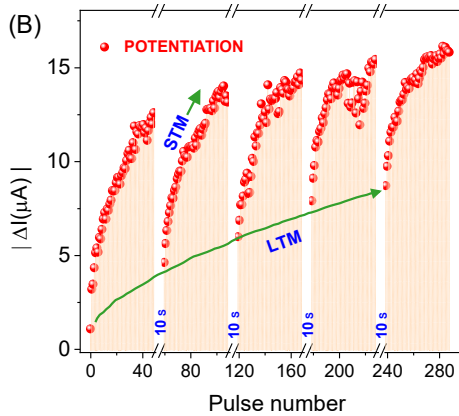
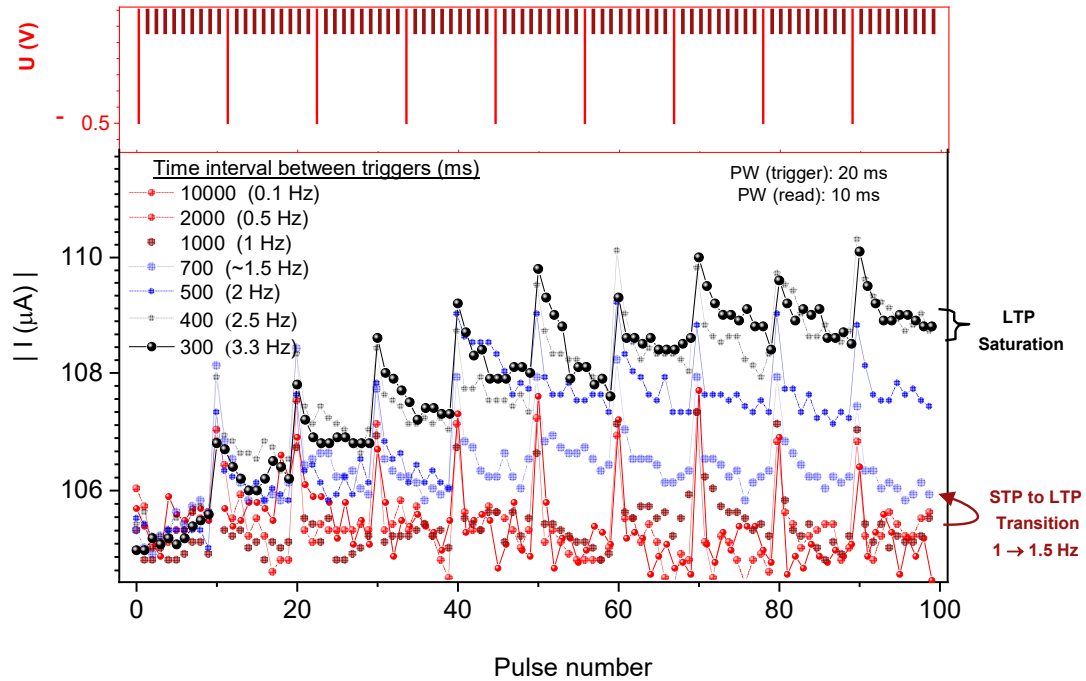


Fig. S7: A) Progression in conductance emulating STP and LTP controlled by distinct stimulation frequencies ranging from 0.1-3.3 Hz, implying a different time interval between two triggers (Δt). Following each program pulse, the current was monitored using 10 successive reading pulses. The upper panel displays the schematics of triggers and read applied. B-C) Illustration of STM vs. LTM evolution, and STF vs. LTF progression across 5 cycles characterized by 50 potentiation and 50 depression-only pulses, interspaced with 10 s intervals. ($\Delta t = 20$ ms).

H. Pavlovian Learning Algorithm: Stimulus-responsive Paradigm

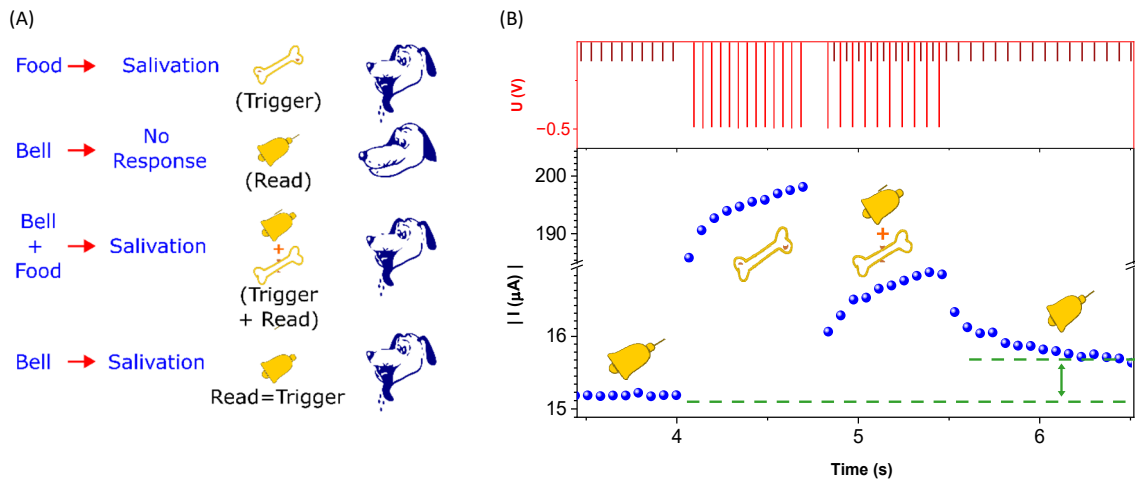


Fig. S8: A) Schematic of the Pavlovian learning algorithm utilized to stimulate dog's learning behavior using conditioned stimulus (bell ringing) and presence of food as the neural reaction (unconditioned stimulus) to create an efficient response (salivation) after repeated pairing with conditioned stimulus, and B) experimental observation of the conditioned and unconditioned results in ITO | PCaPMA | Au device with the trigger as conditioned response. The experiment was carried out on the electrode active area of 0.15 mm².

The stimuli-responsive training in dogs carried out by Pavlov (Fig. S6A) was mimicked using our memristive device with the standard potentiation parameters (Fig. S6B top panel). The stimulation was carried out with the very low magnitude trigger pulses of -0.5 V, while the associated results were recorded using a read pulse (-50 mV, 50 ms). Similar experiment was carried out by Kumar M., et al., in ZnO | Ag-dot | Si device, however the amplitude of trigger used was 3V.¹ The conditioning with significant potentiation was achieved just by 10 sequential trigger pulses indicating a potential to mimic the learning of an artificial synapse such as in visual recognition or directional hearing algorithm with proper sensitivity.

I. Simulation of Paired-pulse Facilitation/Depression (PPF/D)

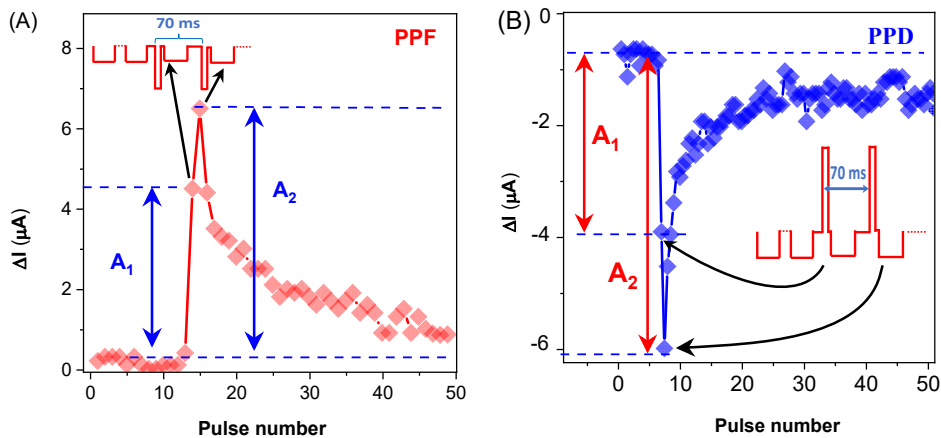


Fig. S9: A-B) Illustration of synaptic potentiation and depression modulation through paired-pulse facilitation (PPF) and pair-pulse depression (PPD), respectively. Synapse responses were illustrated by pairs of temporally synchronized program pulses, and the amplitudes of resultant post-synaptic currents: A_1 and A_2 , were probed by read pulse after the first and second pre-synaptic pulse (pulse with 5 ms), respectively. An inter-spike interval time of 50 ms was maintained. The pulse schematics are shown in the insets.

J. Barrier Height Calculation:

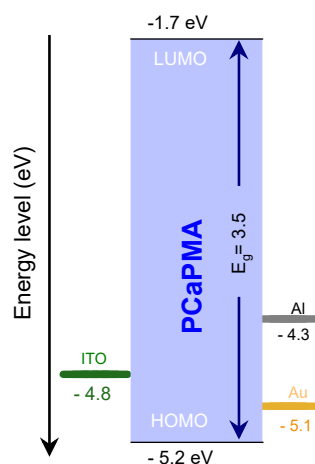


Fig. S10: Energy band-diagram of the ITO | PCaPMA | Au or Al devices.

The work function of aluminum (Φ_{Al}),² gold (Φ_{Au}),³ and ITO (Φ_{ITO}),⁴ to be -4.3, -5.1 and -4.8 eV, respectively, are taken from the literature. Using these values the Schottky energy barrier between metal work function and energy levels of PCaPMA is calculated as below:

Table S1: Calculation of Schottky barrier

Interface	Schottky Barrier (eV)	Interface	Schottky Barrier (eV)
Aluminum/ HOMO	0.9	Aluminum/LUMO	2.6
Gold/HOMO	0.1	Gold/LUMO	3.4
ITO/HOMO	0.4	ITO/LUMO	3.1

K. *In-situ* Raman Spectroscopy under Applied Voltage

Raman spectra were measured with and without applied electric field in sandwiched sample with Raman laser passing through glass | ITO side setting the current compliance of 10 μ A to prevent the device breakdown. The cosmic peaks were removed from the spectra, but no baseline correction was applied. The spectra showed the formation of fluorescence band with the applied field. The intensity of the luminescence evolves also and is dependent on several parameters – apart from the applied voltage and current, it is very likely dependent also on the duration of these specific conditions as well as on the duration of the applied excitation light.

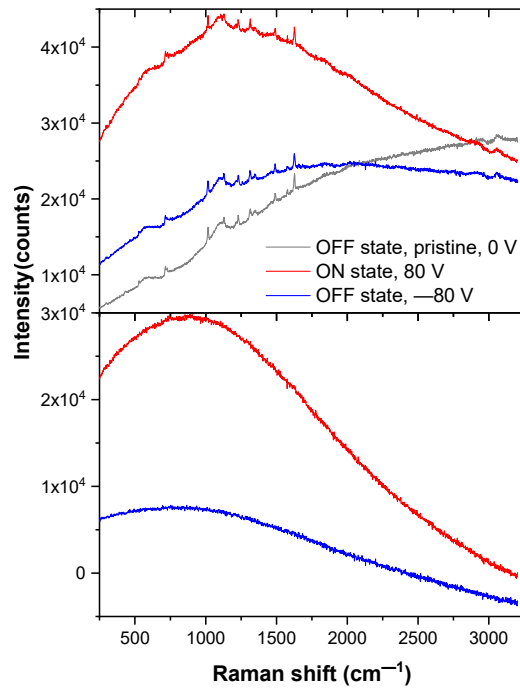


Fig. S11: Upper panel: *In-situ* Raman spectra obtained with excitation laser wavelength of 488 nm on glass | ITO | PCaPMA (550 nm) | Al device (laser through glass | ITO) under applied electric field in the order of 0 V (grey line), + 80 V (red line) and -80 V (blue line), and current compliance of 10 μ A. Lower panel: As in upper panel, but the *in-situ* Raman spectra are displayed after subtraction of a spectrum of pristine sample (sample with the applied voltage of 0 V).

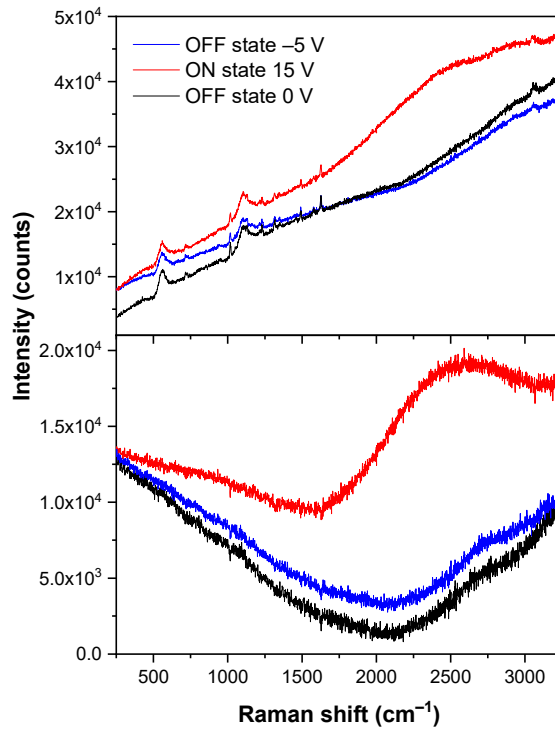


Fig. S12: Upper panel: *In-situ* Raman spectra obtained with excitation laser wavelength of 532 nm on glass | ITO | PCaPMA (175 nm) | Al device (laser through glass | ITO) under applied electric field in the order of 0 (grey line), + 15 (red line) and -5 V (blue line), and current compliance of 100 nA. Lower panel: Difference *in-situ* Raman spectra obtained by a subtraction of a spectrum of sample with 0V voltage applied (pristine).

L. *In-situ* Fluorescence Emission Spectroscopy under Applied Voltage

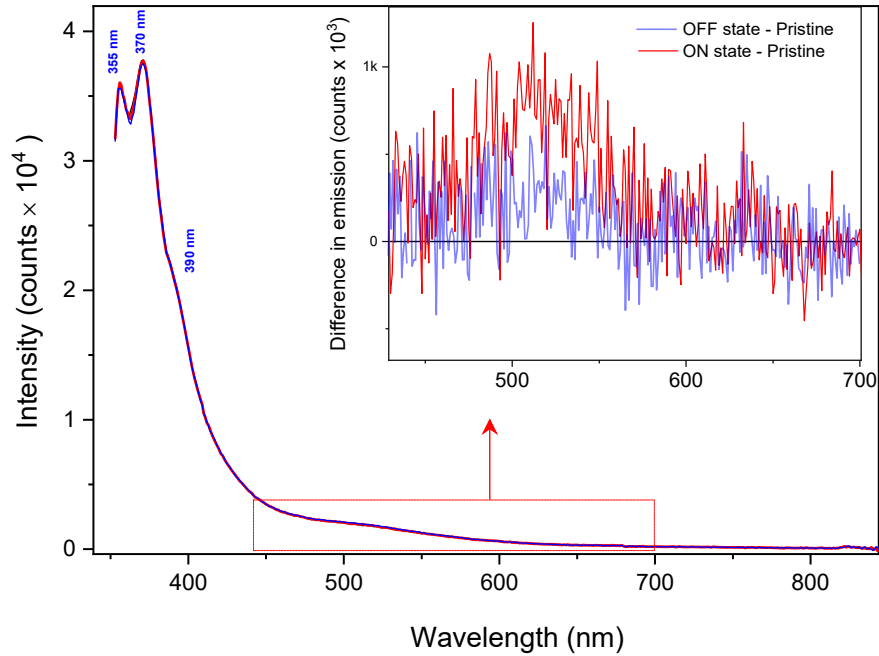


Fig. S13: *In-situ* fluorescence spectra obtained with excitation wavelength of 333 nm on glass | ITO | PCaPMA | Al device (laser through glass | ITO) under applied electric field in the order of 0 (black line), +9 V (red line) and -5 V (blue line), setting the current compliance of 10 μ A. Inset shows the difference *in-situ* fluorescence spectra obtained by a subtraction of a spectrum of voltage applied and pristine sample.

REFERENCES

- 1 M. Kumar, S. Abbas, J. H. Lee and J. Kim, *Nanoscale*, 2019, **11**, 15596–15604.
- 2 E. W. J. Mitchell and J. W. Mitchell, 2006, 372–385.
- 3 W. M. H. Sachtler, G. J. H. Dorgelo and A. A. Holscher, *Surf. Sci.*, 1966, **5**, 221–229.
- 4 T. M. Brown, J. S. Kim, R. H. Friend, F. Cacialli, R. Daik and W. J. Feast, *Appl. Phys. Lett.*, 1999, **75**, 1679–1681.